10

Development of Miniature Microwave Components by Using High Contrast Dielectrics

Elena Semouchkina
Michigan Technological University
USA

1. Introduction

Modern communication systems require microwave components of high performance and small size. In particular, microstrip components are always in demand because of low profile and lightweight. However, despite of many advances, microstrip component miniaturization still remains challenging. One of the ways to solve this problem is to introduce capacitive loading or stepped impedance in the device design. Capacitive loads of different types were often employed in monopole and patch antennas to reduce their dimensions (Lacey et al., 1996; Delaveaud et al., 1998). Stepped impedance (Sagava, 1997) has been also frequently used in resonators, including microstrip ones. For example, stepped impedance approach was used in the design of open-loop filter, in which the microstrip width gradually increased toward the slot that resulted in reduced size and wider upper stop-band (Hong & Lancaster, 1997). Size reduction and improvement of characteristics of an open-loop filter was also reported for filters when symmetrically located patches and open stubs were added in the design (Banciu et al., 2002). However, the efficiency of stepped impedance is limited by the maximum possible size of additional microstrip or patch sections. Another option for device miniaturization is using higher permittivity dielectric substrates. However, this approach meets serious problems, such as impedance mismatch and increased mutual coupling between components.

This Chapter describes an efficient way for microwave component miniaturization and parameter optimization by engineering device substrates with local inclusions or layers of higher permittivity dielectrics to provide local compression of the electromagnetic wave. Such approach utilizes the advantages of higher permittivity materials for miniaturization and parameter tuning, while simultaneously providing solutions for impedance matching and coupling problems. The Chapter outlines the materials and the strategy for their combination that were used to achieve miniaturization and enhanced device functions. A general concept that has been applied is to choose the optimal locations of high and low dielectric constant materials within the structure in accordance with the simulated electromagnetic field distributions at frequencies of device operation. Full-wave electromagnetic modeling has been used to develop device designs.

Low Temperature Co-fired Ceramic (LTCC) technology, which is efficient for fabrication compact multilayer microwave components and packages (Nishigaki et al., 1985), provides the means to co-process diverse ceramics in multilayer and planar architecture. Today several types of ceramic materials, such as columbites (having the relative dielectric permitivity K equal to 20), low-loss glass ceramics (K in the range 17 to 85) (Kniajer et al., 1997), and Bi-pyrochlore (K between 40 to 150) (Kamba et al., 2001; Youn et al., 2002) are ready for integration in the modules based on commercial LTCC tapes with K in the range from 4.1 to 10, either by embedding into the cavities in the substrate or by thin-or thick-film technologies. These achievements in materials offer a possibility to use hybrid dielectric substrates in microwave devices. Technological solutions and examples of prototypes are presented in the Chapter, with emphasis on device modeling and design, prototype processing methods, fabrication tolerance issues, and electrical test results.

The Chapter starts from consideration of open-loop microstrip square ring band-pass filters. Such filters are known to provide elliptical function response notable due to narrow pass band and low insertion loss (Hong & Lancaster, 1995). The Chapter demonstrates that local wave compression due to strategic capacitive load placement enables altering the center and attenuation pole frequencies, the shape and width of the pass-band, and input impedance of the filter by modification of selected resonant modes. Capacitive loading with higher permittivity dielectrics is shown to be very efficient in decreasing the filter size. Different possibilities for designing narrow-band filters comprised of capacitively coupled resonators are demonstrated and prototypes of highly miniaturized filters are described. The examples of filters fabricated by using the LTCC-technology with dimensions decreased by a factor of four compared to unloaded devices are presented, in particular, a band-pass filter with the dimensions of (4.1 x 5.6) mm^2 for the center frequency of 2.45 GHz.

Novel design opportunities for microstrip band-pass filters built on layered substrates of ceramic dielectrics having different permittivities are then demonstrated on the example of a filter for UHF band. A miniature LTCC-filter of (3.6 x 2.8) mm^2 size for the center frequency of 750 MHz, *i.e.*, the frequency chosen for TV broadcasting to cell-phones in Europe, is described.

Finally, the Chapter presents a novel ultra-compact microstrip patch antenna with circular polarization of radiation built on the substrate composed of high contrast dielectrics. The engineered design targeted miniaturization and desired electric characteristics, mitigation of surface wave leakage, recovering of fringing fields and ease of fabrication. Prototype devices made from commercially available high permittivity powders and standard LTCC systems are described.

2. Miniaturization of Microstrip Filters Based on Open-Loop Ring Resonators

2.1 General Design Approach

Here we describe the strategy for the placement capacitive loads in a microstrip resonator to modify selected resonance modes and monitor transmission characteristics. First, open-loop microstrip resonators with capacitve loads placed at different locations are modeled and field distributions at resonance frequencies, as well as transmission spectra of the resonators, are simulated (Semouchkina et. al., 2003).

Fig. 1 shows the geometries of several single-section microstrip open-loop square ring resonators: (a) without any loading so that the structure is composed of only the matrix

dielectric with the relative permittivity K_1 and (b-d) with capacitive loads utilizing high permittivity dielectrics (K_2 and K_3) placed at three different locations: (b) near the slot, (c) in the middle of the front rib and (d) at the side ribs.

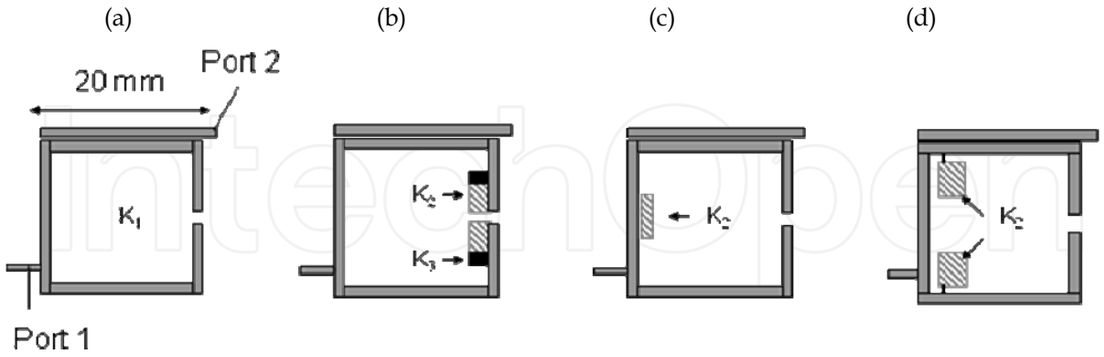

Fig. 1. Schematics of open-loop square ring resonators: (a) without capacitive loading, (b) with loading near the ring slot, (c) with loading in the middle of the front rib, and (d) with loading at the side ribs.

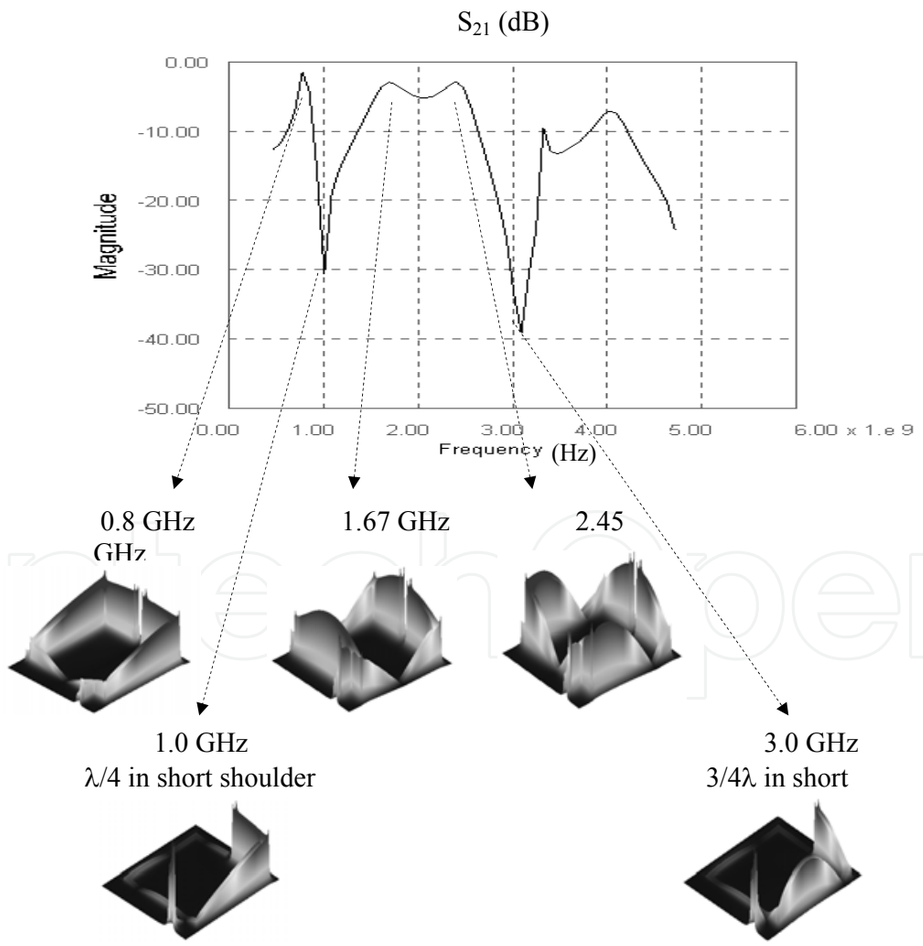

Fig. 2. S_{21} spectrum of open-loop square ring resonator depicted in Fig. 1a, and standing wave patterns corresponding to the peaks and attenuation poles of the spectrum.

The substrate has a thickness of 0.66 mm and a dielectric constant of 9; the width of the microstrips is 1 mm. The loads are either stepped impedance sections of a patch type placed on top of a uniform substrate or metal patches placed above the inclusions of higher-K inside the low-K substrate (as shown in Figs. 1b-d). In the case depicted in Fig. 1b, dielectric inclusions consist of two parts with different K values, with the higher-K (K_2) sections placed closer to the slot than the lower-K (K_3) sections. The resonator shown in Fig. 1d has patch sections separated from the side ribs by a 0.8 mm gap, and connected with them by 0.4 mm wide microstrips. An output microstrip line is added to the rings in order to model the coupling with the next section and to calculate the S_{21} spectrum.

The Finite-Difference Time Domain (FDTD) simulations have been used to simulate transmission and reflection characteristics of the resonators, as well as field distributions in the resonator substrates at different frequencies.

The simulated S_{21} spectrum of the unloaded resonator (see Fig. 1a) is presented in Fig. 2, which also shows the standing wave patterns of the normal electric field component at the frequencies corresponding to the $\lambda/4$, $\lambda/2$ mode and $3/4\lambda$ resonant modes, respectively. It is also seen in Fig. 2 that the first attenuation pole in the S_{21} spectrum at 1 GHz corresponds to the $\lambda/4$ resonance in the right shoulder of the square ring between the input feedline and the gap, while the second pole at 3 GHz is associated with the $3/4\lambda$ resonance in the same shoulder.

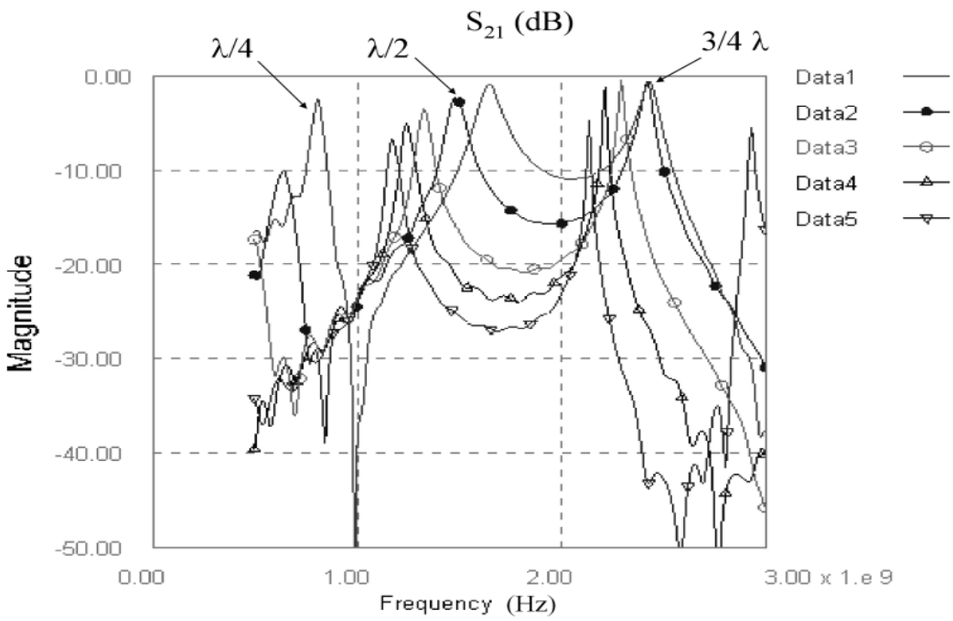

Fig. 3. S_{21} spectra for resonators: (Data1) without loading and (Data2-5) with capacitive load located near the slot (Fig. 1b), (Data2)-loading by metal patches with matrix dielectric (K_1), (Data3)-loading by patches above inclusions with $K_2=K_3=21$, (Data4)-loading by patches above inclusions with $K_2=45$ and $K_3=21$, and (Data5)-loading by patches above inclusions with $K_2=90$ and $K_3=21$.

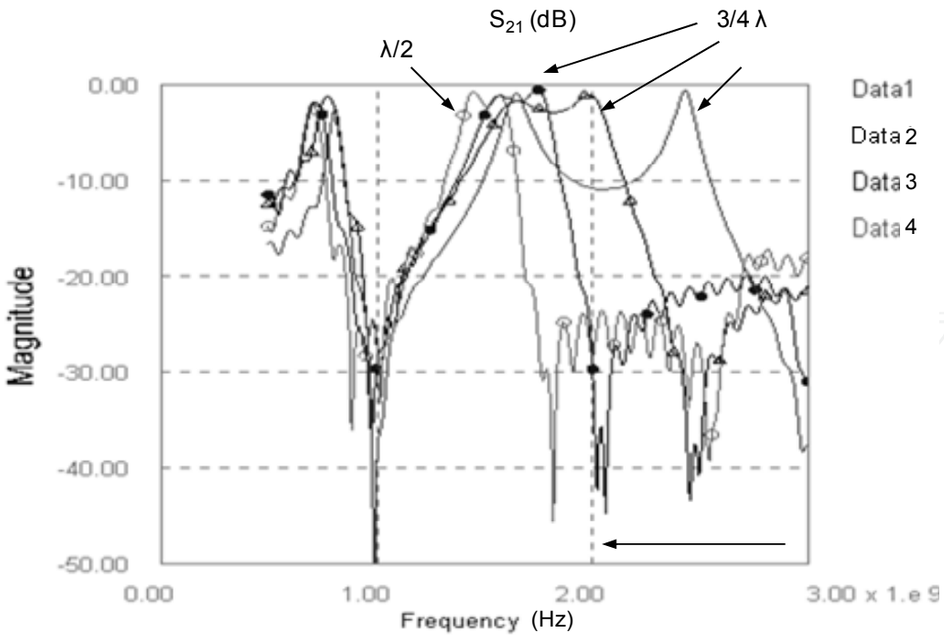

Fig. 4. S_{21} spectra for resonators: (Data1) without loading and (Data2-5) with capacitive load located at the side ribs (Fig. 1d); (Data2)-loading by metal patches; (Data3)-loading by patches above inclusions with K=21; (Data4)-loading by patches above inclusions with K=30

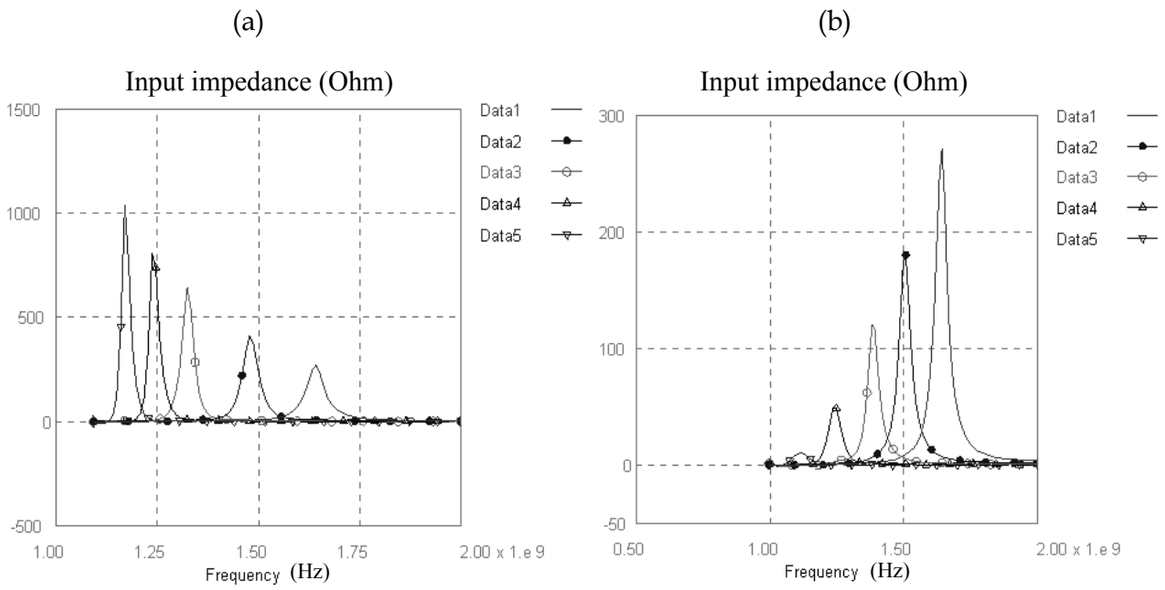

Fig. 5. Input impedance spectra for resonators with capacitive load located: (a) near the slot (Fig. 1b), area of each patch-15 mm², (Data1-Data5) correspond to the same loading as in Fig. 3; and (b) in the middle of the front rib (Fig. 1c) with a patch area of 12 mm²; (Data1)-unloaded filters, (Data2)-filter loaded with capacitor patch with matrix dielectric (K_1=9), (Data3)-capacitor patch with K_2=21, (Data4)-capacitor patch with K_2=45, and (Data5)-capacitor patch with K_2=90.

In order to decrease the resonant frequency of a particular mode of the microstrip resonator, capacitive loads are placed in a position of amplitude maximum of electric field for this mode. Conversely, capacitive load placed at the node of electric field standing wave of a resonant mode does not affect the resonant frequency of this mode. Thus resonant frequencies and transmission zeros can be independently manipulated by selectively loading high-K dielectrics within a low-K matrix structure. For the loading of the type shown in Fig. 1b, the resonant frequencies of all the modes depicted in Fig. 2 decrease, which results in shifting of the entire S_{21} spectrum to lower frequency (Fig. 3). Therefore, this type of loading can be used for the device miniaturization.

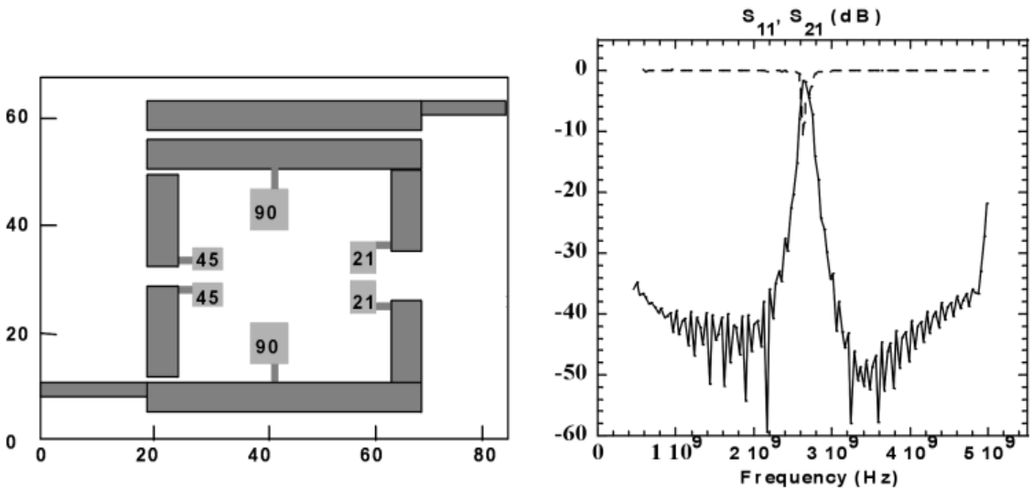

Fig. 6. (a) Geometry (dimensions are given in numbers of cells, the size of one cell is 0.2 mm) and (b) S_{11} (dotted curve) and S_{21} (solid curve) spectra of the filter with the substrate of K=9 loaded by a combination of dielectric inclusions with K=21, 45 and 90.

When the load is located in the middle of the front rib (Fig. 1c), it affects the $\lambda/2$ and λ modes in a similar way but does not alter the $\lambda/4$ and $3/4\lambda$ modes. Quite opposite, the loads placed at the locations of standing wave antinodes for the $3/4\lambda$ mode at the side ribs of the filter (Fig. 1d) strongly affect this mode and the mode responsible for the second attenuation pole, while producing negligible effect on the $\lambda/4$ and $\lambda/2$ modes (compare field patterns in Fig. 2). As the result, strong shifts of the $3/4\lambda$ peak and of the second attenuation pole can be observed in the S_{21} spectrum (Fig. 4). These data illustrate the possibility to modify the widths of the pass- and stop-bands, as well as their shapes, by affecting only selected modes of the spectrum through using proper load location.

Fig. 5 demonstrates changes in input impedance of the resonator due to the loading: input impedance increases for the loading shown in Fig. 1b (see Fig. 5a), while its behavior is opposite (Fig. 5b) for the loading shown in Fig. 1c. It points at the possibility to match impedance by varying the location and the permittivity of the loads.

It is worth noting that capacitive loads connected precisely to the points where the resonant mode has electric field maxima (see Fig. 1d), were found to be more efficient in modifying the resonant frequency of the mode and the input impedance, than adding stepped impedance sections in the areas of high electric fields (Figs. 1b, c).

By using the described startegy, a combination of different loads of higher permittivity than that of the substrate, with their placement governed by the simulated field distribution, can be used to design a filter with reduced size and optimized characteristics. An example of how the loading of initial open-loop square-ring resonator (Fig. 1a) can be optimized to provide a narrow pass band at 2.45 GHz is presented below. Instead of the passband of $\lambda/4$ mode of the initial resonator, which is not accompanied by a low frequency attenuation pole (Fig. 2), the pass band between 1.5 GHz and 2.5 GHz, which results from the $\lambda/2$ and $3/4\lambda$ modes, can be used to form two attenuation poles in the transmission spectrum. Fig. 6a depicts the schematic of a one-section filter with the relative substrate permittivity of 9, in which the size and the permittivity of the loads placed at the front and back ribs were adjusted to provide the center frequency of 2.45 GHz and to match input impedance, the loads at the side ribs were used to shift the $3/4\lambda$ mode closer to the $\lambda/2$ mode, and additional slots in the microstrip ring were introduced to suppress undesirable modes. The size of this filter is (10 x 10) mm^2 compared to (20 x 20) mm^2 of an unloaded resonator (Fig. 1a), and the S_{21} spectrum (Fig. 6b) exhibits a narrow pass band.

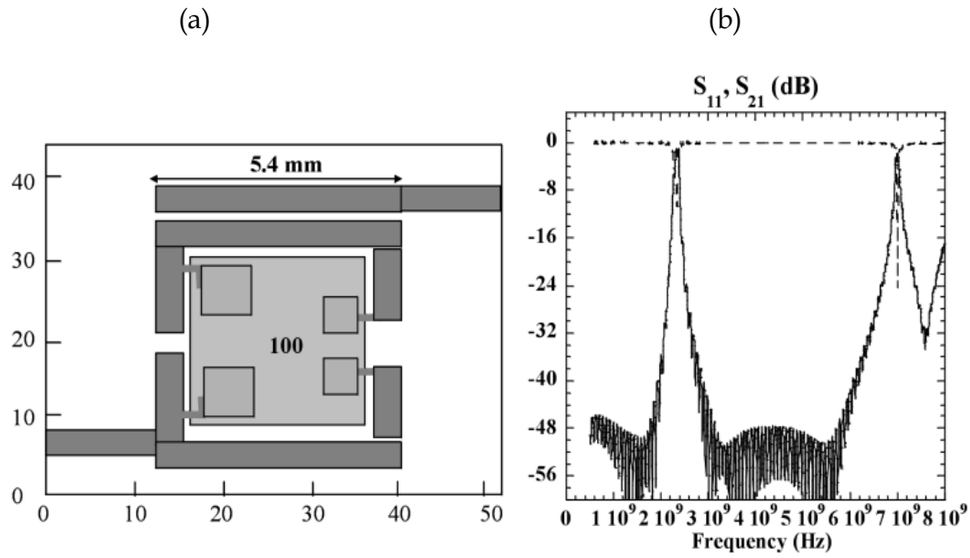

Fig. 7. (a) Geometry and (b) S_{11} (dotted curve) and S_{21} (solid curve) spectra of the filter with the substrate of K=7.8 and thickness of 660 microns loaded by a dielectric plug with K=100.

Combining loads of different permittivity offers potentially many degrees of freedom in shaping the pass-band, however, it is technologically difficult to reproduce. The design example presented in Fig. 7a demonstrates that efficient pass-band shaping and size reduction of the filter could be achieved even when only one type of high–K dielectric is used for loading. In this design, one plug of K=100 is inserted in the substrate of K=7.8 within the microstrip loop. Metal patches and parts of the connecting strips are located at the surface of the plug to provide local loading. The simulated S-parameter spectra of this filter show no spurious modes up to frequencies three times higher than the center one, and the pass-band of 3.6% (Fig. 7b), while its area is decreased from (20 x 20) mm^2 for an unloaded resonator down to (5.4 x 5.4) mm^2.

2.2 Realization of Filters with Local Loading by High-Permittivity Materials

For practical realization of filters with hybrid dielectrics, either high-K superstrate layers over low-K substrates or high-K plugs embedded into low-K substrates could be emplemented (Semouchkina et. al., 2004; Semouchkina et. al., 2005). The examples below describe the development of designs and approaches for the fabrication of a miniature microstrip filter for 2.45 GHz center frequency with a narrow band and low insertion loss in the pass-band.

In the design depicted in Fig. 8a, a square-shaped superstrate layer with the area slightly less than the area inside the ring is placed on top of the substrate. Metal patches located at the top and the bottom of the superstrate serve as the electrodes of the loads, and the bottom electrodes are connected to the ground through vias in the substrate. The substrate thickness is 660 microns, and its permittivity is 7.8. The superstrate is 55 microns thick and has the permittivity of 100. The size and the locations of the electrodes of the loads are adjusted to provide the central frequency of the filter equal to 2.45 GHz. To improve the pass-band characteristics, two open-loop resonators with 3.75 mm side are combined, and the coupling gap between them is optimized to provide low return loss level and symmetric slopes of the S_{21} spectrum Fig. 8b).

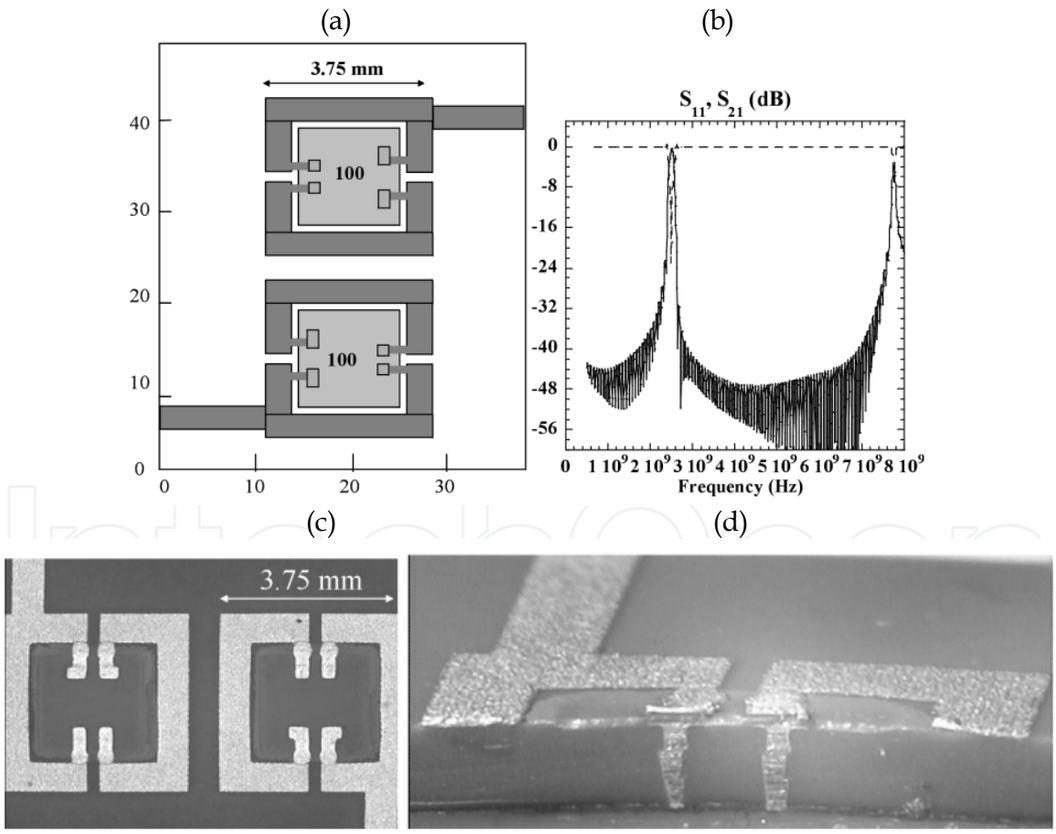

Fig. 8. (a) Geometry and (b) S_{11} (dotted curve) and S_{21} (solid curve) spectra of the filter with the substrate of K=7.8 and thickness of 660 microns loaded by superstrate with K=100 and thickness of 55 microns; (c) top and (d) cross sectional views on the prototype with the superstrate layer.

The latter design was reproduced with the substrate made of three layers of DuPont 951 commercial LTCC tape (K=7.8). To make via-connection between the bottom electrodes of the loads and the ground, the tapes were punched with a 150-micron punch and then the holes were filled with silver via fill. The ground plane was printed on the backside of the lower layer with filled vias using commercial silver ink. Bottom electrodes of the loads and microstrip pattern were printed on the top layer using commercial silver ink. The superstrate was then printed on this electroded tape using Bismuth Pyroclore ink, and the top electrodes of the loads were printed on top of the superstrate using silver ink. Bottom layer with ground plane and filled vias, middle layer with filled vias and top layer with electroded superstrate were stacked, collated and laminated. Filters were then singulated and fired to 875°C peak temperature for 30-minute dwell time. Top and cross-section views of the prototype are shown in Figs. 8c, d. However, in the described prototype, the expected value of dielectric constant of 100 was not achieved for the printed superstrate apparently due to the interaction between the superstrate material and the conducting ink. As the result, the measured resonance frequency of the filter exceeded the targeted 2.45 GHz and corresponded to a superstrate having the dielectric constant of 49 that was confirmed by the independent measurements on fabricated capacitors.

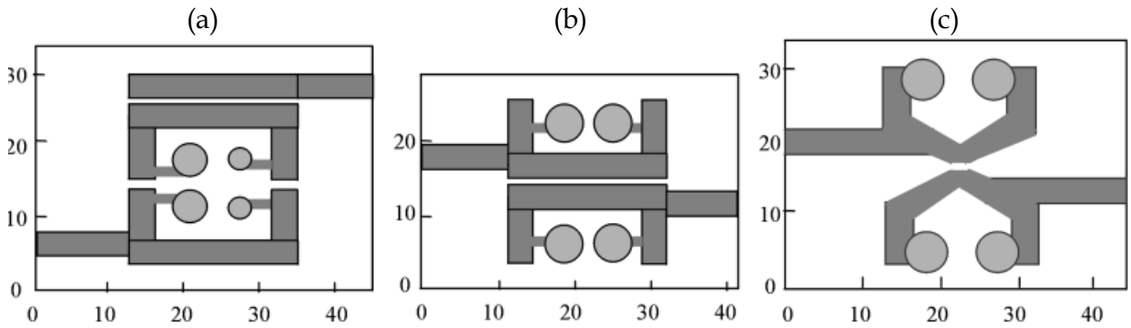

Fig. 9. Geometries of filters with substrates of K=7.8 and high-K plugs of K=74 immersed in the holes punched in the substrate.

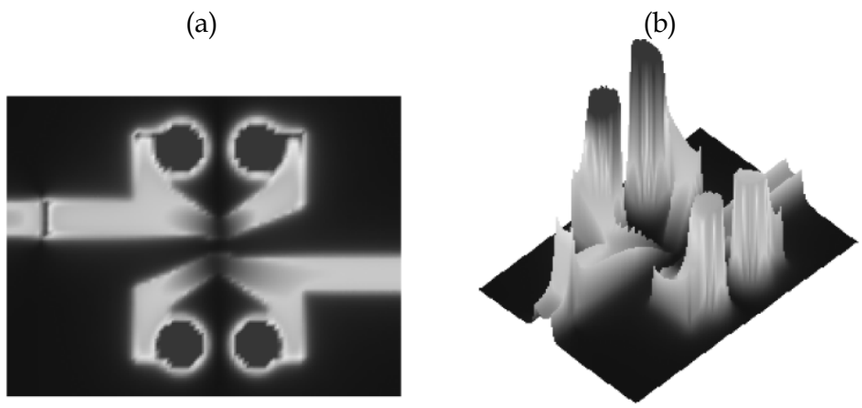

Fig. 10. (a) Contour plot and (b) 3D distribution of the electric field in the resonator depicted in Fig. 9c at the frequency 2.45 GHz.

Therefore, another fabrication approach, i.e. to embed plugs made of preliminary prepared high-K ceramic tape into a low-K substrate, has also been applied. For this purpose, three layers of DuPont 951 LTCC tape with dielectric permittivity of 7.8 and the thickness of 250 microns each have been used as the substrate material, while the 250 microns thick Bismuth Zinc Tantalate (BZT) LTCC tape with K=74 and $Q \approx 400$ (at 2.45 GHz) (Kamba et al., 2001; Youn et al., 2002) - as the material for plugs to be inserted in the top substrate layer. Fig. 9 illustrates the transformation of the filter design in the process of its adjustment to the fabrication opportunities.

Fig. 9a shows the initial design of a one-section open-loop resonator utilizing four round high-K pugs of 1.06 mm diameter with various diameters of the plug electrodes that provides the resonance frequency of 2.45 GHz. In order to simplify the processes of plug insertion and metallization, in the "back-to-back" design depicted in Fig. 9b, one half of the ring is flipped over and four equal plugs with completely metallized top and bottom surfaces are used. This design provides a stronger magnetic coupling between the half-rings, in difference from the design in Fig. 9a, in which the half-rings are coupled primarily via electric field in the coupling gaps.

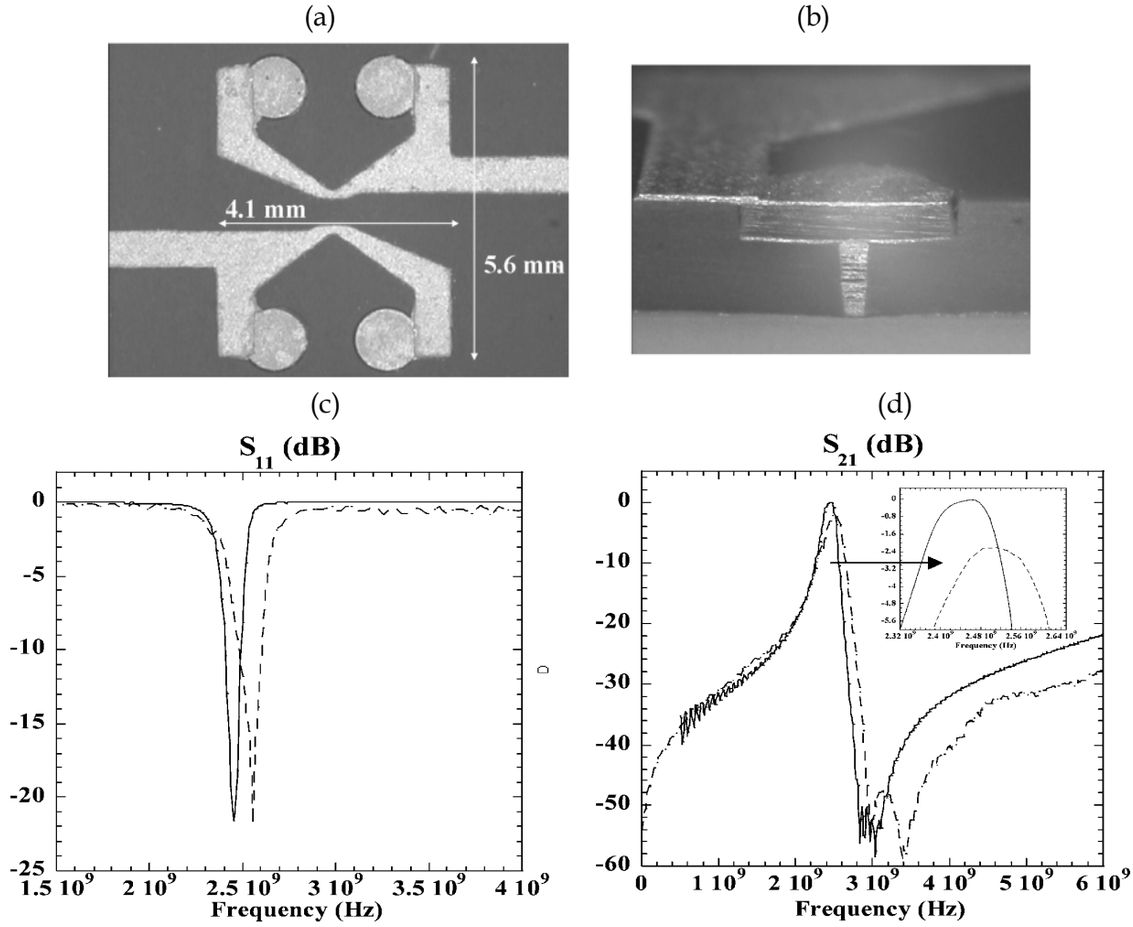

Fig. 11. (a) Top and (b) cross sectional views on the prototype with high-K plugs in the low-K substrate; and simulated (solid curves) and experimentally measured (dotted curves) (c) S_{11} and (d) S_{21} of the prototype.

Equal size of loading capacitors (Fig. 9b), however, does not provide sufficient degrees of freedom in optimizing the resonator characteristics. Therefore, in the final design shown in Fig. 9c, the shapes of the microstrips and the locations of the feedlines have been additionally adjusted. Fig. 10 shows the distribution of electric field normal component in the plane located below the substrate surface at the resonant frequency of 2.45 GHz, which points at half-wavelength resonance in the two half-rings at this frequency. The presented design consists of two resonators and is a two-pole (second order) filter with an asymmetric characteristic. Asymmetric insertion loss responses with one attenuation zero are often observed for multi-pole filters with one way for signal propagation, when none of the resonators is bypassed or cross-coupled (Amary et al., 2003). A second attenuation zero in such filter could be added by introduction cross-coupling in the filter design.

The prototype fabrication started with preparation vias by punching holes with the diameter of 150 microns in the two bottom substrate layers, and filling them with silver via fill ink. Then the top layer was punched using a 1.25 mm diameter punch. The three substrate layers were laminated in a platen press to form a "tray" for subsequent plug insertion, and PEOX „glue" was used to promote layer adhesion (Wilcox & Oliver, 2002). This lamination technique has been employed so that hole integrity could be maintained. BZT tape was printed on both bottom and top sides with silver ink and then punched using a 1.25mm punch. The resulting metallized BZT plugs were then pressed into slots formed in the LTCC tray. The filled tray was laminated and microstrip pattern was then printed using silver ink. Resonators were singulated and fired to peak temperature of 850°C for 30 minutes holding time. Air dried silver (Premetek 1228) was painted on the backs of the samples to form the ground plane.

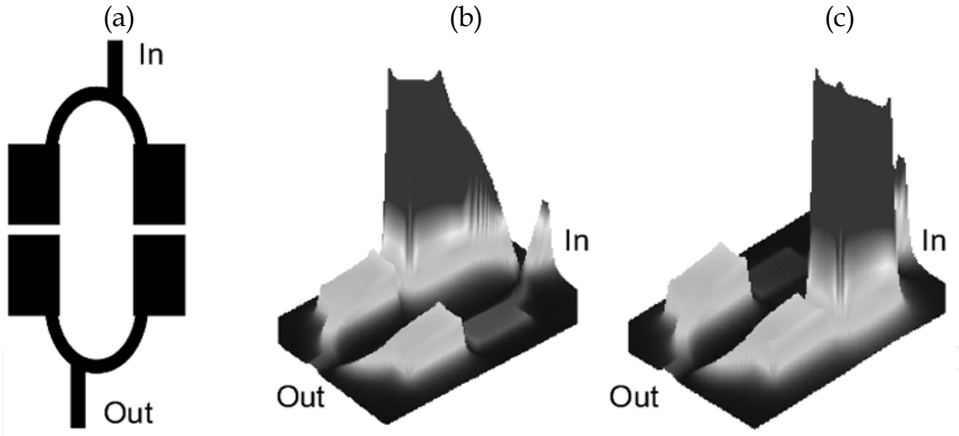

Fig. 12. (a) Schematic of the filter with double-coupled „horse-shoe" resonators and standing wave pattern of the normal electric field component in the vicinity of (b) the frequency of the lower transmission zero and (c) the frequency of the upper transmission zero.

Figs. 11a, b present top and cross-sectional views of the fabricated prototype. Inclusion of high permittivity dielectric, as well as a via connecting the bottom electrode of the plug with the ground, are clearly seen. Figs. 11c, d compare the simulated and measured S-parameters of the prototype. The achieved return loss level in the pass band agrees with the predicted value (-22 dB), which indicates that the input impedance of the prototype has been matched. The measured value of the center frequency is 2.50 GHz, which, in comparison with the simulated value of 2.45 GHz, corresponds to an error of 2 %. The measured insertion loss

level of (–2.23 dB) demonstrates that losses introduced by high-K plug insertion are small. It is worth noting that the main circuitry of the device is still located at the low-K substrate that decreases the influence of possible losses connected to high-K materials. The dimensions of the fabricated prototype are just (4.1 x 5.6) mm².

In real production environment, the tolerances on the material properties and the manufacturing process could require tuning of the narrow filter band, which depends on the capacitance of the inserted high-K loads. Taking into account that upper electrodes of the loads are located at the surface, this capacitance could be tuned by using fine laser trimming of the top electrodes. Metal removal with 50 microns accuracy will allow for resonant frequency shift by about 30 MHz at each trimming step.

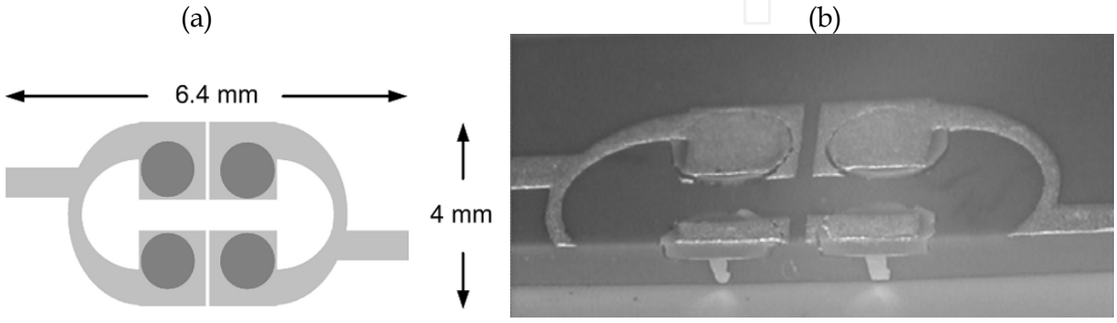

Fig. 13. (a) Layout of the filter loaded by high-permittivity plugs; and (b) cross-sectional view of the filter prototype showing high-permittivity dielectric plugs inserted into a commercial LTCC matrix. Vias connect metalized plugs to the ground plane at the bottom of the structure.

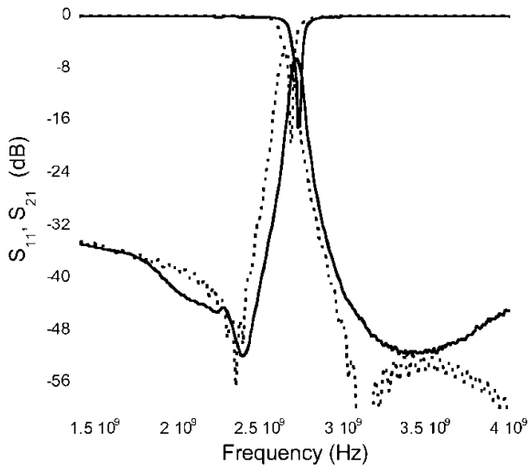

Fig. 14. Comparison of the measured S_{11} and S_{21} of the filter prototype depicted in Fig. 13b (solid curves) with the simulated ones (dashed curves).

In order to provide a second attenuation zero in the insertion loss response of the filter, a double-coupled design consisting of "horse-shoe" resonators has been developed (Hennings et. al., 2003; Hennings et. al., 2004; Hennings et. al., 2006). Fig. 12 presents the schematic of such filter and standing wave patterns of electric field in the substrate at the frequencies of

the transmission zeros. As seen from Figs. 12 b, c; two quarter-wavelength resonances take place in either one of the shoulders of the input resonator, while the field amplitudes drop down to almost zero in the other shoulder.

To miniaturize the filter shown in Fig. 12a with the dimensions (7.68 x 12.61) mm², a design having cylindrical plugs of high-permittivity dielectric located in the LTCC substrate underneath rectangular patches has been developed (Semouchkina et. al., 2005b). Fig. 13a presents the layout of this filter with the size of (4.0 x 6.4) mm², while Fig. 13b shows the cross-sectional view of the prototype fabricated using the described above LTCC based approach and the same materials. The presented in Fig. 14 simulated and measured S-parameter spectra demonstrate that the filter's pass-band has two attenuation zeros. Thus dimensions of the filter have been decreased by a factor of 4 compared to unloaded one by using local insertion of higher permittivity dielectrics.

3. Development of Miniature Filters for TV Broadcasting Band by Using Layered Substrates of Mixed Ceramic Dielectrics

3.1 Novel Filter Design with Double-Coupled Stepped Impedance Resonators

In many cases, there is a need for such filter transfer functions, which include a number of transmission zeroes. In particular, the zeroes are used to sharpen the transitions between the pass-band and the rejection-band regions. The transmission zeroes can be realized by providing multiple signal paths in cross-coupled structures (Hong & Lancaster, 1996) or adding a signal bypass between input- and output-ports (Amari, 2001). Alternative methods are described by (Hennings et. al., 2006; Belyaev et. el., 2001). Multilayer LTCC-filters described in literature are mainly designed for WLAN applications, e. g. (Lin et. al., 2006), and have rather broad bandwidth. In some cases, they suffer from low out-of-band rejection or exhibit unwanted spurious resonances. Moreover, several LTCC-filters succumb to high complexity and contain a big number of metallized LTCC-layers. In order to simplify the fabrication process, the quantity of metallized layers, vias, and dielectric layers should be kept low.

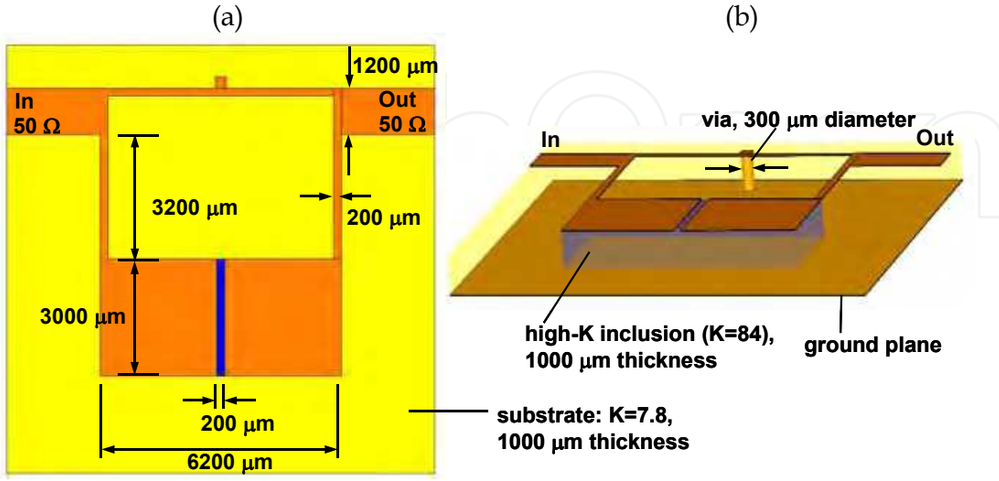

Fig. 15. Microstrip filter using mixed dielectrics: (a) top view, (b) perspective view.

Here, the development of a miniature narrow-band LTCC-filter with high performance but low degree of complexity is described (Hennings et. al., 2007). In order to retain small dimensions, only two-pole filters built of two quarter-wavelength resonators have been designed. The center frequency of the pass-band is 750 MHz, *i.e.*, the frequency chosen for TV broadcasting to cell-phones in Europe. It is worth noting that a DVB-H network is expected to be soon provided in the USA by using frequencies near 700 MHz. Therefore, small-size high-quality filters for UHF band are expected to get high priority.
The design of the filter employs stepped impedance microstrip resonators loaded by plugs of high permittivity underneath wide metal patches. Fig. 15a depicts the initial design consisting of two end-coupled quarter-wavelength stepped impedance resonators placed in parallel normally to the feed lines. A high-K plug is shown inserted in a low permittivity matrix in Fig. 15b. Simulations have been performed for dielectric constants of the matrix of 7.8, and of the plug of 84. The thickness of the plug was the same as one of the matrix, *i.e.*, 1 mm. The filter was designed to be mounted on an additional substrate, or, if necessary, another low-K layer could be placed on top of the structure to ensure material adhesion.

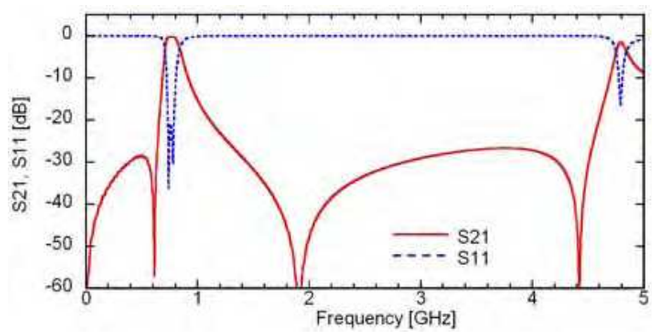

Fig. 16. Simulated S-parameters for the filter shown in Fig. 15.

The via seen in Fig.15b has the diameter of 300 microns and is used to connect the circuit to ground and to serve as shunt-inductance, providing for inductive coupling between the resonators, while capacitive coupling is achieved through the narrow gap (200 microns) between the patches of the two resonators. Without the via, the two quarter-wavelength resonators would merge to an open loop half wavelength resonator which could support only a single fundamental resonance (Semouchkina, 2003), while with the via, two fundamental modes could be supported in the filter. In comparison with filters based on open loop resonators (Semouchkina et. al., 2003; Semouchkina et. al, 2005a), the new design allowes for obtaining the desired two-pole filter characteristics at more compact filter dimensions.
The use of mixed inter-resonator coupling is advantageous due to desirable possibility for capacitive and inductive coupling to compensate each other (Belyaev et. al, 2001; Hong & Lancaster, 2001), and to allow for obtaining transmission zeroes at frequencies located closely to the filter pass-band edge. Such compensation allows one to achieve a weak overall coupling coefficient that is required for a narrow band-width. Depending on the dimensions of the gap and the via, either capacitive or inductive coupling is dominant at center frequency. At the given in Fig. 15 dimensions, capacitive coupling was found to exceed inductive coupling, although the latter was meaningful. A design with pure capacitive coupling would have required a much wider gap between the patches to make coupling weak at employment the same high-K plug located underneath the coupled patches of the resonators.

The area consumption of the filter is (6.2 x 7.4) mm² = 45.88 mm² for the dimensions scaled for the center frequency of 0.75 GHz. The simulated S-parameter spectra of the novel filter design are displayed in Fig. 16. As seen from the figure, the filter characteristics look very promising and could be additionally improved at careful balance of capacitive and inductive coupling. In fact, lower transmission zero is observed very close to the pass-band edge. In modified filters with dominant inductive coupling other transmission zero was similarly close to the opposite pass-band edge.

However, since both the electric and the magnetic coupling coefficients in the described above design are relatively high, the weak overall coupling coefficient appeares to be sensitive to the parameter choice. In addition, further miniaturization requires increased capacitive loading of the resonators, and, so, thinner plugs of the high-K material. As processing of the plugs is relatively complicated, a modified design is presented below, which has a thin planar layer of high permittivity material inserted in the LTCC matrix instead of local plugs and multilevel metallization to employ this layer for capacitive loading.

3.2 Realization of Multilayer LTCC Filters

Figs. 17a through 17d illustrate the filter design based on three-layer LTCC sandwich-like substrate (low-K, high-K, low-K) having 3 x 90 microns height.

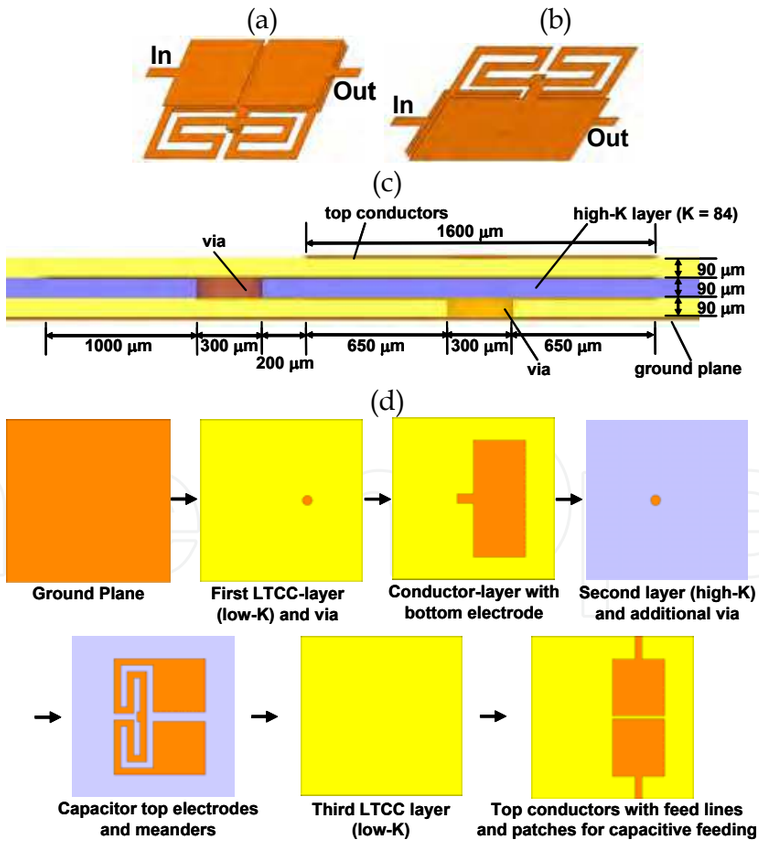

Fig. 17. Filter design: (a) and (b) perspective views with hidden substrate and ground plane, (c) cross sectional view, and (d) design schematics (top view).

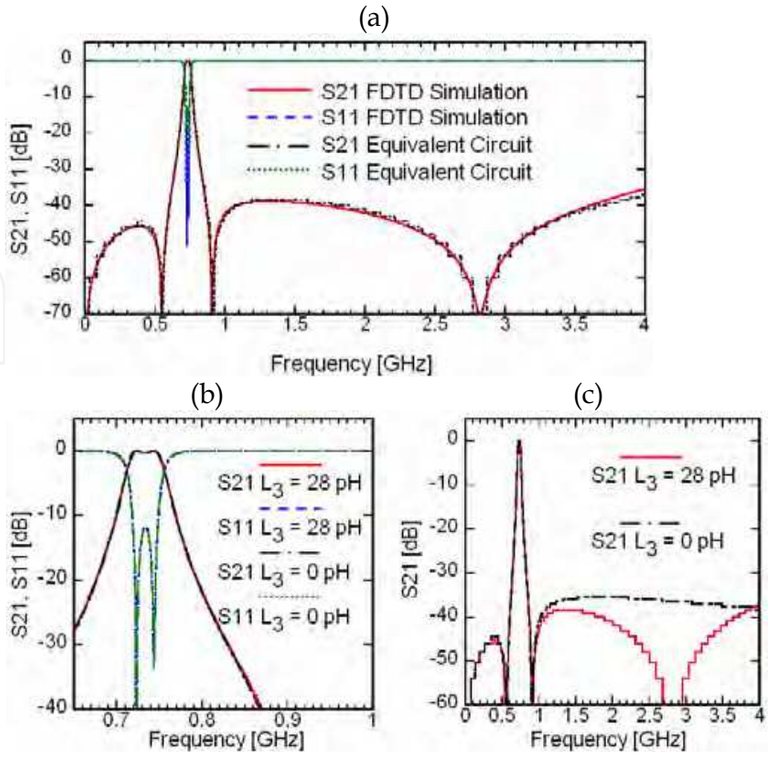

Fig. 18. (a) Comparison of simulated S-parameters for filter shown in Fig. 17 and calculated S-parameters for equivalent circuit. (b), (c) S-parameter spectra for the equivalent circuit in case of $L_3 = 0$ and $L_3 = 28$ pH.

In the new design, capacitively loaded low-impedance sections of two resonators are replaced by capacitors formed by using interlayer metallization. These capacitors have common bottom electrode, which is connected to ground plane by an additional via. Instead of straight microstrips used in the design depicted in Fig. 15, the space-saving meander lines are employed to connect top electrodes of the capacitors to via providing for inductive inter-resonator coupling. In the new design, the gap between the capacitors of two resonators is increased, and, therefore, the contribution of capacitive coupling is essentially decreased in comparison with the previous design. The resonators are fed capacitively (without a direct ohmic contact to feedlines) by using additional patches located just above the resonator capacitors on the upper substrate surface. The gap between these top patches is quite narrow to enable capacitive bypass path, which is known to cause a pair of transmission zeroes if applied to two inductively coupled resonators. This implementation with quasi-lumped elements allowes for scaling the dimensions down to (3.6 x 2.8) mm² = 10.08 mm² at the center frequency of 0.735 GHz.
As seen in Fig. 18a, excellent characteristics with transmission zeroes near the pass-band edges have been obtained in FDTD simulations. The 3-dB bandwidth is as low as 6 %, and spurious bands occur at frequencies more than 7.9 times higher than the center frequency.
In order to get a deeper insight into the filter performance it was modeled by a lumped element equivalent circuit shown in Fig. 19. Here, the two resonator capacitors are represented by elements C_1, the capacitance between their common bottom electrode and

the ground plane - by element C_3, whereas L_3 is related to the inductance of the via connecting this electrode to ground. The elements C_2 describe capacitive feeding, C_4 - capacitive bypass, and L_2 and C_5 - inductive and capacitive inter-resonator coupling. The meanders are represented by inductors L_1, and their associated parasitic capacitances - by elements C_6. The element values have been first roughly approximated and then gradually changed up/down to the levels providing for better coincidence of the calculated filter characteristics to the results of the FDTD simulations. The same filter characteristics could be realized by various combinations of element values, in particular, for an equivalent contour with neglected C_6 and values of C_1 and C_2, corresponding to ideal parallel plate capacitors. We have used the following values of these and other elements: C_1 = 21.82 pF, C_2 = 2.03 pF, C_3 = 4.43 pF, C_4 = 30 fF, C_5 = 370 fF, C_6 = 0, L_1 = 1.86 nH, L_2 = 115 pH, L_3 = 28 pH. As seen in Fig. 18a, the chosen values allowed for correct describing of the bandwidth, ripples, and the rejection performance of the filters. It means that physical design of the filter was close to an ideal lumped element circuit within the considered frequency range, while the impact of parasitic elements could be compensated by appropriate parameter choice. Introduction of C_6 values in consideration has shown that the impact of these parasitics was relatively small. They could slightly reduce the resonant frequency and increase the external Q factor. The element C_5 compensated only a small part of the inductive inter-resonator coupling. The capacitor C_3 was found to be negligible. It had only a minot impact on the frequency of the third transmission zero at 2.82 GHz, which was found to be related to the presence of the inductor L_3 (representing the via).

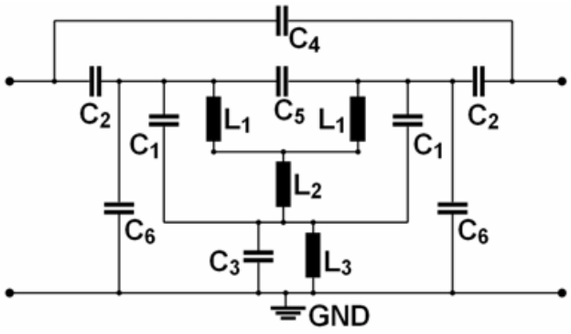

Fig. 19. Equivalent circuit of the Filter shown in Fig. 17.

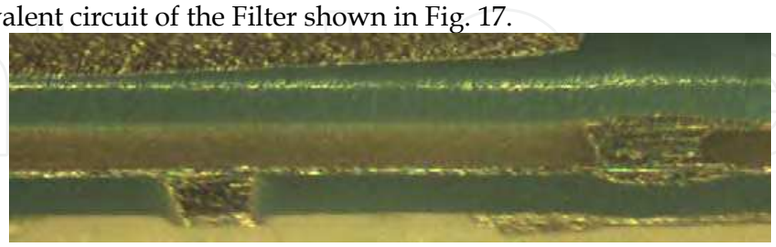

Fig. 20. Cross-section of fabricated sample with high K layer and vias.

Comparison of the filter characteristics obtained at different values of L_3 is shown in Figs. 18b and 18c. As seen from the figures, the element L_3 is useful for enhancement of the rejection band performance without affecting the pass-band characteristics. This holds as long as L_3 does not exceed the order of magnitude of the value based on physical estimations (28 pH). It is also worth mentioning that the inductor L_3 does not cause any

significant loss contribution, even if this element has a very low Q-factor. Hence, it is not critical. However, the presence of the elements C_3 and L_3 in the circuit causes an appearance of a spurious band at frequencies beyond 13 GHz. If this is undesirable, while the enhanced rejection at about 2.8 GHz is not necessary, then the filter design could be modified through complete removal of both the via and the lower LTCC layer.

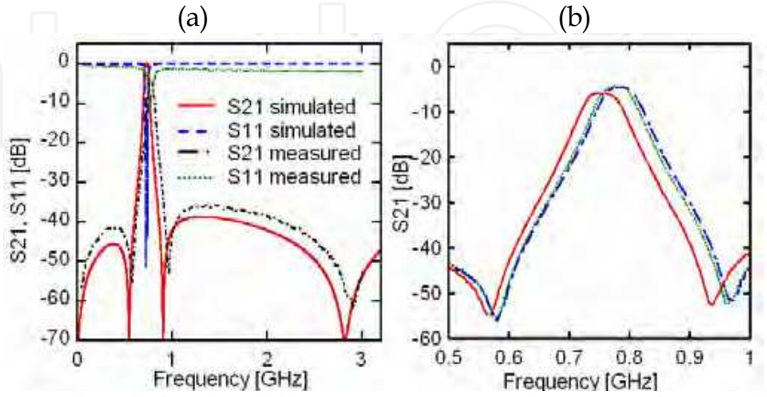

Fig. 21. (a) Measured and simulated S-parameter spectra in comparison. (b) Measured S21-spectra of three different samples.

The prototypes have been fabricated by using the layout given in Fig. 17. Metallization was provided by silver inks designed for LTCC technology. The upper and lower layers were made by using the LTCC DuPont 951 tape (the permittivity K=7.8). The middle layer was made by using the BZT tape (K =60-84). First, vias were punched and filled in layer 1 (low K), and layer 2 (high K). Then, the ground plane was printed on the backside of layer 1 and dried at 80°C. Next, the rectangle pattern was printed on topside of layer 1. After it, the meander including pattern was printed on backside of layer 3. Finally two patches with feed lines were printed on topside of layer 3. The layers were aligned and laminated using 3000 psi at 70 C for 15 minutes. Filters were singulated and fired at 850 C for 30 minutes dwell time. Fig. 20 presents the cross-section of one of the prototypes.
The results of measurements in comparison with the results of simulations are shown for one of the samples in Fig. 21a. The S-parameter spectra of the prototype agree well with the simulated results. Fig. 21b shows the measured results for three different samples, which demonstrate good repeatability of the fabrication process.
The described data confirm that employment of quarter wavelength resonators and layered substrates of mixed dielectrics allows one to develop highly miniaturized quasi-lumped LTCC-filters with excellent characteristics. In comparison to other LTCC-filters, they benefit from narrow bandwidth, reduced complexity and lower volume, since only three LTCC-layers are used.

4. Wearable Patch Antenna for Voice Communications with Substrate Composed of High Contrast Dielectrics

4.1 Designing Miniature Patch Antenna with CP

Future communication systems will require small and low cost antennae. It is especially true for wearable antennae for voice communications. However, small antenna size becomes a

severe problem in UHF band due to large resonance length of the antenna patch. The most direct way of reducing antenna dimensions is employment of substrates with high dielectric permittivity. However, such substrates cause narrow antenna bandwidth, impedance matching problems, transfer energy into substrate waves, and decreased fringing fields that leads to low efficiency (Zhang et. al., 1995; Hoofar & Perrotta, 2001; Hwang et al., 2003).

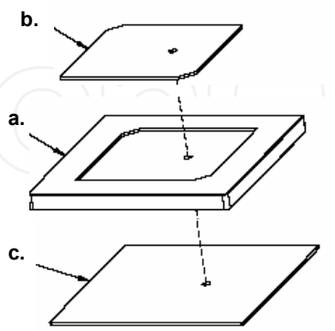

Fig. 22. Schematic diagram of a typical patch antenna for 915 MHz: (a) dielectric dlock, (b) patch, and (c) ground plane. Size of device is roughly 80 by 80 by 5.5 mm.

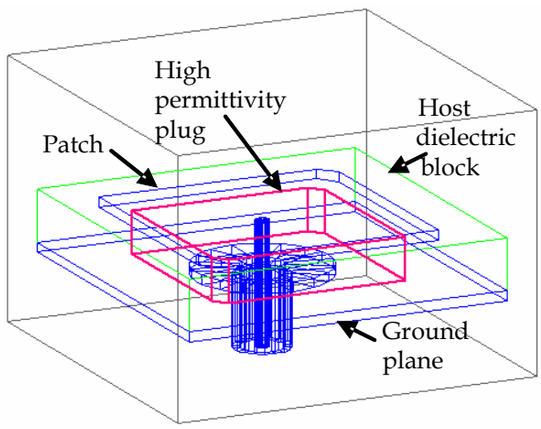

Fig. 23. Simulation model of the miniaturized antenna.

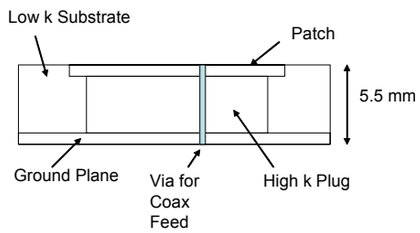

Fig. 24. Schematic cross-section of a miniaturized antenna with capacitive loading of the patch. Antenna area has been decreased by about 80%.

To mitigate these drawbacks, the antenna designers have explored various approaches. In particular, superstrates of higher permittivity with or without parasitic radiators are recommended for recovering the gain loss (Hwang et. al., 2003; Teo et. al., 2000). In order to recover the antenna bandwidth, it was proposed (Kiziltas et al., 2003) to employ textured substrates with optimized distribution of several high contrast materials. However, such

texturing is difficult for practical realization. Another well known method to increase antenna bandwidth is the employment of thicker substrates. However, it enhances surface modes generation. Although several solutions for suppressing surface wave leakage have been considered, most of them lead to increasing antenna dimensions. To mitigate surface wave generation, it was proposed (Kula et al., 2004) to truncate high permittivity substrates near the patch edges. In (Semouchkina et. al., 2002) it was earlier shown that truncation of high index dielectrics by low permittivity plugs significantly obstructs surface waves propagation.

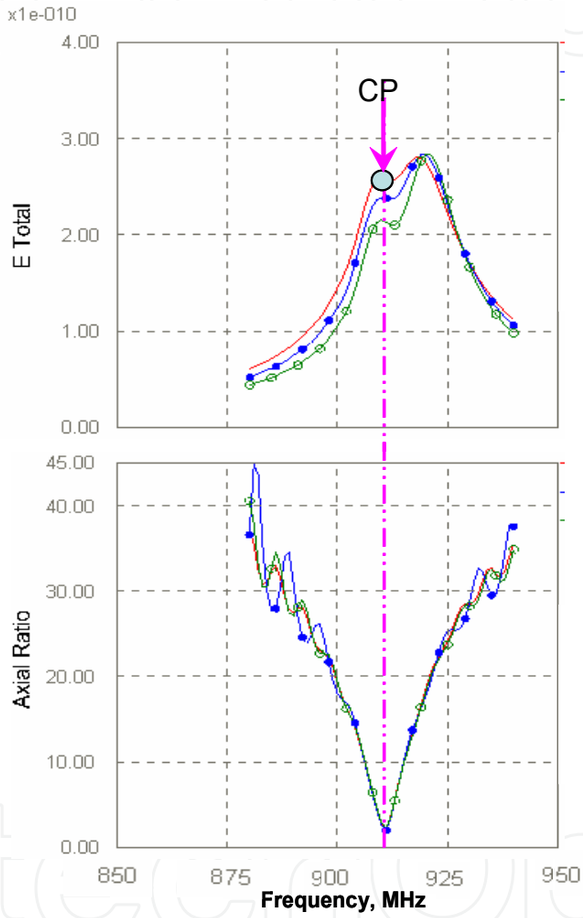

Fig. 25. Simulated spectra of radiation efficiency (upper plot) and axial ratio (lower plot) for antennas with optimized patch, plug, and cut corner dimensions; three curves correspond to a slightly differnt feed point locations.

In order to avoid drawbacks of higher permittivity substrates, it was proposed (Lee & Harackiewicz, 2002) to use partially filled substrates, with high permittivity dielectric bars placed in areas of high electric fields and with other areas filled with air. While this approach could be helpful to solve narrow bandwidth and low gain problems of antennas based on high permittivity substrates, it could not prevent fringing fields deterioration. An opposite proposed approach was to place high permittivity substrate underneath the antenna patch everywhere excluding the regions with peak radiation and fields (Chen &

Volakis, 2005). High permittivity substrate regions of the substrate were partly removed in proportion with electric field intensity and replaced by low permittivity dielectric. While antenna prototypes demonstrated high gain and bandwidth broadening, the graded design was not convenient for practical realization, and circular polarization (CP) could not be achieved.

A new approach to the development of a miniature microstrip patch antenna with CP based on employment of antenna substrates of high contrast dielectrics is described below (Semouchkina et al., 2007). The design targeted miniaturization and desired electric characteristics, mitigation of surface wave leakage, recovering of fringing fields and ease of fabrication.

As a starting point, conventional microstrip patch anttenas designed for operation at 915 GH have been analyzed. These antennas generally use alumina substrate having dimensions of (80 x 80) mm^2 and a thickness of 5.5. mm. Patches are designed with cut corners to provide elliptical polarization. A schematic diagram of this type of antenna is shown in Fig. 22. Far-field radiation measurements confirmed that radiation patterns of these antennas were close to spherical with backward radiation intensity of about 3 dB less than the forward intensity and peak gain of about 1.5 dBi. They had split or wide radiation efficiency peak and axial ratio exceeding 5 dB. This antenna serves as a basis for the integration of higher permittivity material to achieve antenna miniaturization without performance deterioration.

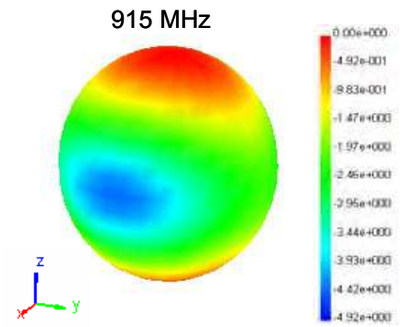

Fig. 26. 3D far-field radiation pattern of the novel antenna at the resonance frequency.

The conventional design is modified by inserting a square plug of higher permittivity material into the lower permittivity block substrate. The plug dimensions are smaller than the patch dimensions so that the fringing field distortion is mitigated. At the same time, capacitive loading of the patch by the high permittivity plug allowes for compressing of the resonance wavelengths inside the plug. Plug dimensions and permittivity are optimized to get maximal possible miniaturization while maintaining antenna operation frequency of 915 MHz and preserving strong friging fields to provide high antenna efficiency. CP of radiation is achieved by using plugs with properly cut corners and a precise feed location. The 3D model used in FDTD simulations is shown in Fig. 23. As seen from the figure, antenna feed is modeled by a coax cable. Its outer conductor is connected with the ground plane, and inner conductor - with the patch through a via in the plug. The perfectly matched (PML) boundary conditions are used at the second end of the coax to mitigate reflections. The antenna is excited by the current launched from the inner conductor of the coax.

Materials used in the model of the antenna included high permittivity ceramic powders of K = 84 for plug fabrication, and LTCC material systems with the relative permittivity of 7.4 for

the fabrication of the host dielectric block. By employing the high permittivity material under the patch, the overall dimensions of the new antenna design were decreased to 35 by 35 mm, about one fifth the size of the conventional antenna. A schematic diagram of the miniaturized device is shown in Fig. 24. According to simulations the antenna efficiency was not degraded from miniaturization and the new design had a wider bandwidth. The results of simulations of the total electric far-field and the axial ratio are given in Figs. 25, while the 3D far-field pattern at the resonance frequency is presented in Fig. 26. As seen from the figures, the antenna radiates in zenith despite of the small ground plane and is capable of providing for axial ratio at the levels essentially less than 3dB at the resonance frequency.

4.2 Miniature Antenna Fabrication

The prototypes of the novel antennas have been fabricated by using ceramic technologies. Dupont 951 LTCC material has been used for fabrication of the low permittivity dielectric block and Ferro COG820MW was chosen for fabrication of the high permittivity plug.

Plugs fabrication starts with pressing a large rectangular slab at 16,000 psi using the Ferro COG powder coated with 3% acryloid binder. A template of the plug is generated using a drawing program. A factor of 1.226 should be applied to the template to account for shrinkage of the ceramic after firing. The template of the plug is placed on the slab, and the shape is cut from the soft green ceramic. The coax feed hole is drilled into the plug. The plug is then fired at a peak temperature of 1330^{o}C. After firing, plugs are further machined on a grinding wheel to their final size. Dupont 6160 silver paste is applied to the front and back of the plug and dried.

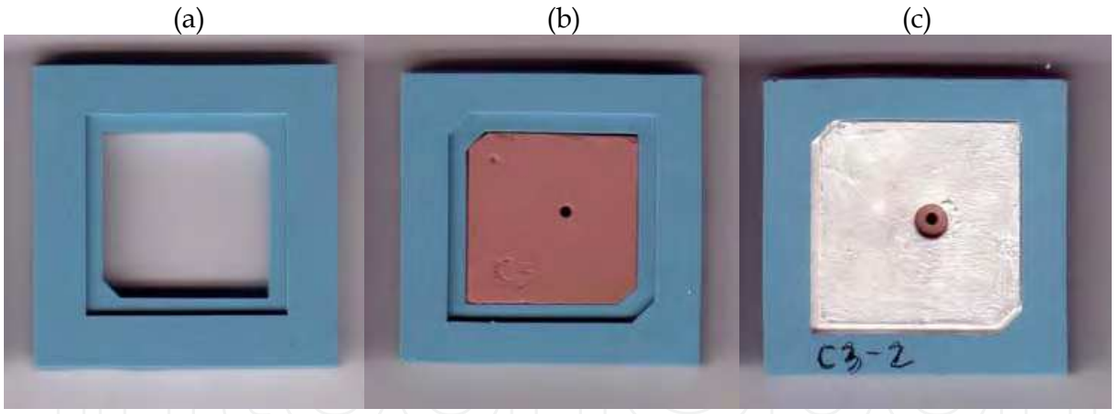

Fig. 27. Antennas are shown in process: (a) Low-K dielectric block, (b) dielectric block fired around the high-K plug, before final metallization is applied, and (c) finished miniaturized antennas with metallized LTCC patch with via for coax feed. Final size is 35 by 35 mm.

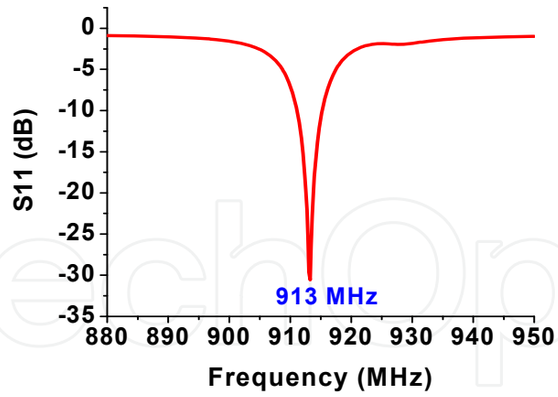

Fig. 28. Measured S_{11} spectrum of the miniaturized antenna

The host dielectric substrate block is fabricated from 50 layers of Dupont 951 LTCC. To build up the thickness, several layers of the LTCC should be first isostatically laminated at 70°C, 3000 psi for 10 minutes. The resulting 1 mm thick LTCC stacks are then punched to provide the open area for plug insertion. A shrinkage factor of 1.14 should be applied to this open area so that during firing the LTCC would shrink around the inserted plug. Metallization is printed onto the green layers using Dupont 6145 silver paste. Each punched LTCC stack is painted with a honey/water 75/25 mixture and placed on an alignment fixture. The honey mixture acts as glue between the LTCC layers and eliminates the need of further lamination steps that often result in the distortion and smashing of the soft ceramic devices (Rocha et. al., 2004).

The low permittivity LTCC block is then placed on an alumina setter and the metallized, fired plug is placed in the center of the cut out area in the block. The device is then fired to a peak temperature of 850°C for 30 minutes. The LTCC block substrate material shrunks about 14% to tightly surround and contact the edges of the plug.

Examples of the miniaturized antenna in process are presented in Fig. 27. Fig. 28 demonstrates the measured S_{11} spectrum with a -30dB minimum at the operating frequency of 913 MHz for the miniaturized antenna having the area of only 20% of the area of the original antenna.

5. Conclusion

The potential of high permittivity dielectric materials for local capacitive loading of microstrip components has been demonstrated in this Chapter. Capacitive loads are introduced in the device design based on the analysis of simulated field distribution at resonant frequencies. The use of hybrid dielectrics helps to substantially decrease device dimensions and to shape and optimize all characteristics of the device. The designs of miniature microstrip resonators, filters, and antennas with local high-permittivity dielectric loading have been developed, and the prototypes have been fabricated by using the LTCC technology that allowed for coprocessing different ceramic materials in multilayer and planar architecture. The results of the prototype measurements were found to agree with the simulation results.

6. References

Amari, S. (2001). Direct synthesis of folded symmetric resonator filters with source-load coupling. *IEEE Microwave and Components Letter.*, Vol. 11, pp.264-266

Amari, S.; Tadeson, G.; Cihlar, J. & Rosenberg, U. (2003). New parallel λ/2-microstrip line filters with transmission zeros at finite frequencies, *Proceedings of IEEE Microwave Theory Tech. Int. Symp,*Vol. 1 , pp. 543-547, June 2003

Banciu, M. G.; Ramer, R. & Ioachim, A. (2002). Microstrip filters using new compact resonators. *Electron. Lett.,*Vol. 38, pp. 228-229

Belyaev, B.; Laletin, N. & Leksikov, A. (2001). Coupling coefficients of irregular microstrip resonators and selective properties of filters on their basis, *Proceedings of 2001 IEEE Conf. on Microwave Electronics: Measurements, Identification, Applicatio,* pp. 86-91

Delaveaud, C.; Laveque, P. & Jecko, B. (1998). Small-sized low-profile antenna to replace monopole antenna. *Electron. Lett.,* Vol. 34, No. 8, (Apr. 1998) pp. 716-717

Hennings, A.; Semouchkin, G.; Semouchkina, E. & Lanagan, M.. (2003). Design optimization of microstrip square-ring band-pass filter with quasi-elliptic function, *Proceedings of 33rd European Microwave Conf.*, pp. 175-178, Munich, germany, October 2003

Hennings, A.; Semouchkina, E.; Semouchkin, G. & Lanagan, M. (2004). Novel compact band-pass filters with horse-shoe microstrip resonators, *Proceedings og 34th European Microwave Conf.,* Amsterdam, October 2004

Hennings, A.; Semouchkina, E.; Baker, A. & Semouchkin, G. (2006). Design optimization and implementation of bandpass filters with normally fed microstrip resonators loaded by high-permittivity dielectric. *IEEE Trans. Trans. Microwave Theory Tech.*, Vol. 54, pp. 1253-1261

Hennings, A..; Semouchkina, E.; Baker, A.; Semouchkin, G.; Waser, R. & Lanagan, M. (2007). Development of miniature LTCC filter for TV broadcasting band by using substrates of mixed dielectrics, *Proceedings of 37th European Microwave Conf.,* pp. 866-869, Munich, Germany, Sept. 2007

Hong, J. S. & Lancaster, M. J. (1995). Canonical microstrip filter using square open-loop resonator. *Electron. Lett.,* Vol. 31, pp. 2021-2022

Hong, J. S. &. Lancaster, M. J. (1996). Couplings of microstrip square open-loop resonators for cross-coupled planar microwave filters. *IEEE Trans. Microwave Theory Tech.*, Vol. 44, pp. 2099-2109

Hong, J. S. & Lancaster, M. J. (1997). Theory and experiment of novel microstrip slow-wave open-loop resonator filters, *IEEE Trans. Microwave Theory Tech.,* Vol. 45, pp. 2358-2365

Hong, J. S. & Lancaster, M. J. (2001). *Microstrip Filters for RF/Microwave Applications*, Wiley, New York, pp. 249-251, pp. 73

Hoofar, A. & Perrotta, A. (2001). An experimental study of microstrip antennas on very high permittivity ceramic substrates and very small ground planes. *IEEE Trans.Antennas Propagation,* Vol. 49, pp. 838-840

Hwang, Y.; Zhang, Y. P. & TLo, T. K. (2003). Aperture-coupled microstrip antenna loaded with very high permittivity ceramics", www.interscience.wiley.com, DOI 10.1002/mmce. 10072

Kamba, S.; Porokhonsky, V.; Pashkin, A.; Bovtin, V.; Petzelt, J.; Nino, J.; Trolier-McKinstry, S.; Randall, C. & Lanagan, M. (2001). Broad-band dielectric spectroscopy of Bi pyrochlores in the range 100 Hz – 100 THz, *Proceedings of the COST525 Meeting*, 2001, pp 49-53

Kiziltas, G.; Psychoudakis, D.; Volakis, J. L. & Kikuchi, N. (2003). Topology design optimization of dielectric substrates for bandwidth improvement of patch antenna. *IEEE Trans.Antennas Propagation*, Vol. 52, pp. 2731-2743

Kniajer, G.; Dechant, K. & Apte, P. (1997). Low loss, low temperature cofired ceramics with higher dielectric constants for multichip modules (MCM), *Proceedings of IEEE Int. Conf. On Microchip Modules*, pp. 121-127

Kula, J.; Psychoudakis, D.; Chen, C.-C.; Volakis, J. L. & and Halloran, J. H. (2004). Patch antenna miniaturization using thick truncated textured ceramic substrates, *Proceedings of IEEE AP-S Int. Symp.*, Vol. 4, pp. 3800-3803

Lacey, D.; Drossos, G.; Wu, Z.; Davis, L. E.; Button, T. W. & Smith, P. (1996). Miniaturized HTS microstrip patch antenna with enhanced capacitive loading, *Proceedings of IEE Superconducting Microwave Circuits Colloq.*, Vol. 4, pp. 1-6, Apr. 1996

Lin, K.-C.; Chang, C.-F.; Wu, M.-C. & Chung, S.-J. (2006), Dual bandpass filters with serial configuration using LTCC technology. *IEEE Trans. Microwave Theory Tech.*, Vol. 54, pp. 2321-2328

Nishigaki, S.; Yano, S.; Fukuta, J. & Fuwa, T. (1985). A new multilayered low temperature fireable ceramic substrate, *Proceedings of Int. Hybrid Microelectron. Symp.*, pp.225-234

Rocha, Z.; Garcia, N.; Oliveira, N.;Matos, J. & Gongora-Rubio, M. (2004). Low temperature and pressure lamination of LTCC tapes for meso-systems, *Proceedings of IMAPS Ceramic Interconnect Technology Conference*, pp 205 – 210, Denver Co., April 2004

Sagava, M.; Makimoto, M. & Yamashita, S. (1997). Geometrical structures and fundamental characteristics of microwave stepped-impedance resonators. *IEEE Trans. Microwave Theory Tech.*, Vol. 45, pp.1078-1085

Semouchkina, E.; Semouchkin, G.; Cao, W. & Mittra, R. (2002). FDTD study of surface waves in microstrip and patch structure, *Proceedings of IEEE Microwave Theory Tech. Int. Symp,* pp.1127-1130

Semouchkina, E.; Semouchkin, G.; Lanagan, M. & Mittra, R. (2003). Field simulation based strategy for designing microstrip filters, *Proceedings of IEEE MTT-S Int. Symp.* pp. 1897-1900

Semouchkina, E.; Baker, A.; Semouchkin, G. & Lanagan, M. (2004). Microwave component miniaturization by local embedding high-permittivity dielectric materials in low-permittivity substrates, *Proceedings of 34th European Microwave Conf.,* Amsterdam, October 2004

Semouchkina, E.; Baker, A.; Semouchkin, G.; Lanagan, M. & Mittra, R. (2005a). New approaches for designing microstrip filters utilizing mixed dielectrics. *IEEE Trans. Microwave Theory Tech.*, Vol. 53, pp. 664-652

Semouchkina, E.; Hennings, A.; Baker, A.; Semouchkin, G. & Lanagan, M. (2005b). Miniature filter with double-coupled horse-shoe microstrip resonators capacitively loaded by using high-permittivity material, *Proceedings of 35rd European Microwave Conf.*, pp. 293-296, Paris, France, Oct. 2005

Semouchkina, E.; Baker, A.; Semouchkin, G.; Kerr, T. & Lanagan, M. (2007). Wearable patch antenna for voice communications with substrate composed of high contrast dielectrics, *Proceedings* of *IEEE AP-S International Symposium,* Honolulu, Hawaii, June 2007

Teo, P. T.; Vinoy, K. J.; Jose, K. A.; Varadan, V. K.; Varadan, V. V. & Gan, Y. B. (2000)., Design and development of tunable multi-layer smart antennas using ferroelectric materiasl. *J. Intell. Materials Systems Structures*, Vol. 11, pp.294-299

Wilcox Sr. D. L. & Oliver, M. (2002). LTCC, an interconnect technology morphing into a strategic microsystem integration technology, *Proceedings of the IMAPS Advanced Technology Workshop*, pp. 1-4, Providence, RI, May 2002

Youn, H.-J.; Randall, C.; Chen, A.; Shrout, T. & Lanagan, M. (2002). Dielectric relaxation and microwave dielectric properties of Bi_2O_3-ZnO-Ta_2O_5 ceramics. *J. Mater. Res.,* Vol. 17, pp. 1502-1506

Zhang, Y. P.; Lo, T. K. & and Hwang, Y. (1995). A dielectric loaded miniature antenna for microcellular and personal communications, *Proceedings of IEEE AP-S Int.Symp.*, pp.1152-1155

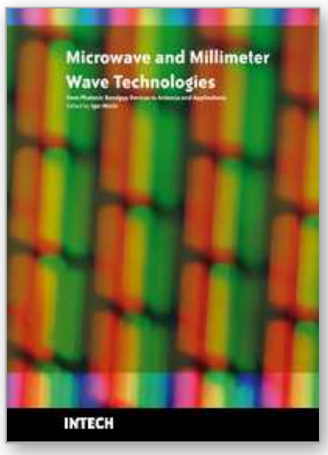

Microwave and Millimeter Wave Technologies from Photonic Bandgap Devices to Antenna and Applications

Edited by Igor Minin

ISBN 978-953-7619-66-4
Hard cover, 468 pages
Publisher InTech
Published online 01, March, 2010
Published in print edition March, 2010

The book deals with modern developments in microwave and millimeter wave technologies, presenting a wide selection of different topics within this interesting area. From a description of the evolution of technological processes for the design of passive functions in milimetre-wave frequency range, to different applications and different materials evaluation, the book offers an extensive view of the current trends in the field. Hopefully the book will attract more interest in microwave and millimeter wave technologies and simulate new ideas on this fascinating subject.

How to reference

In order to correctly reference this scholarly work, feel free to copy and paste the following:

Elena Semouchkina (2010). Development of Miniature Microwave Components by Using High Contrast Dielectrics, Microwave and Millimeter Wave Technologies from Photonic Bandgap Devices to Antenna and Applications, Igor Minin (Ed.), ISBN: 978-953-7619-66-4, InTech, Available from: http://www.intechopen.com/books/microwave-and-millimeter-wave-technologies-from-photonic-bandgap-devices-to-antenna-and-applications/development-of-miniature-microwave-components-by-using-high-contrast-dielectrics

INTECH
open science | open minds

InTech Europe
University Campus STeP Ri
Slavka Krautzeka 83/A
51000 Rijeka, Croatia
Phone: +385 (51) 770 447
Fax: +385 (51) 686 166
www.intechopen.com

InTech China
Unit 405, Office Block, Hotel Equatorial Shanghai
No.65, Yan An Road (West), Shanghai, 200040, China
中国上海市延安西路65号上海国际贵都大饭店办公楼405单元
Phone: +86-21-62489820
Fax: +86-21-62489821

IntechOpen